*Article*

# Owl Neck Spine inspired, Additively Manufactured, Joint Assemblies with Shape Memory Alloy Wire Actuators

**Robin Löffler [1,*], Stephan Tremmel [2] and Rüdiger Hornfeck [1]**

[1] Nuremberg Institute of Technology, Kesslerplatz 12, 90489 Nuremberg, Germany
[2] University of Bayreuth, Universitätsstraße 30, 95447 Bayreuth, Germany
* Correspondence: robin.loeffler@th-nuernberg.de; Tel.: +49-911-5880-1908

**Abstract:** Nature provides plenty of good examples for simple and very efficient joint assemblies. One example is the enormously flexible cervical spine of American barn owls, which consists of 14 cervical vertebrae. Each pair of vertebrae produces a comparatively small individual movement in order to provide a large overall movement of the entire cervical spine. The biomimetic replication of such joints is difficult due to the delicate and geometric unrestricted joint shapes as well as the muscles that have to be mimicked. Using X-ray as well as micro computed tomography images and with the utilisation of additive manufacturing, it was possible to produce the owl neck vertebrae in scaled-up form, to analyse them and then to transfer them into technically usable joint assemblies. The muscle substitution of these joints was realised by smart materials actuators in the form of shape memory alloy wire actuators. This actuator technology is outstanding for its muscle-like movement and for its high energy density. The disadvantage of this wire actuator technology is the low rate of contraction, which means that a large length of wire has to be installed to generate adequate movement. For this reason, the actuator wires were integrated into additively manufactured carrier components to mimic the biological joints. This resulted in joint designs that compensate for the disadvantages of the small contraction of the actuators by intelligently installing large wire lengths on comparatively small installation spaces, while also providing a sufficient force output. With the help of a test rig, the developed technical joint variants were examined and evaluated. This demonstrated the technical applicability of this bionic joints.

**Keywords:** biomimetic innovation; additive manufacturing; shape memory alloys; resource efficiency; sustainability

## 1. Introduction

Additive manufacturing (AM) offers itself as an excellent manufacturing technology for biologically inspired mechanical assemblies [1–4]. All AM technologies have the layered part building process in common. For example, either heat-liquefied plastic is layered on top of each other through a nozzle (Fused Deposition Modeling - FDM), parts are produced by sequentially layering plastic or metal powder in a powder bed and then melting it by laser (Selective Laser Sintering - SLS and Selective Laser Melting - SLM), or resins are selectively cured layer by layer with ultraviolet light (Stereolithography - SLA). In particular, AM stands out from conventional manufacturing techniques due to the great geometric design freedom, the wide variety of materials, the high production speed (rapid prototyping) as well as the constant production costs from a quantity of 1 [5]. It is thus possible, for example, to print biological joints, joint assemblies or bone structures in great detail for analysis purposes [6,7] (Figure 1 (a) - (c)) or to produce bionic designs for technical applications with high mechanical loads [6,8,9] (Figure 1 (d) - (f)). Even the flexible membrane of the spider's leg in Figure 1 (d) is printed using the SLS technology. For highly stressed zones within the components, either thinner wall cross-sections in the form of a topology optimisation or local density differences through different infill

Preprints (www.preprints.org) | NOT PEER-REVIEWED | Posted: 22 February 2023 doi:10.20944/preprints202302.0388.v1

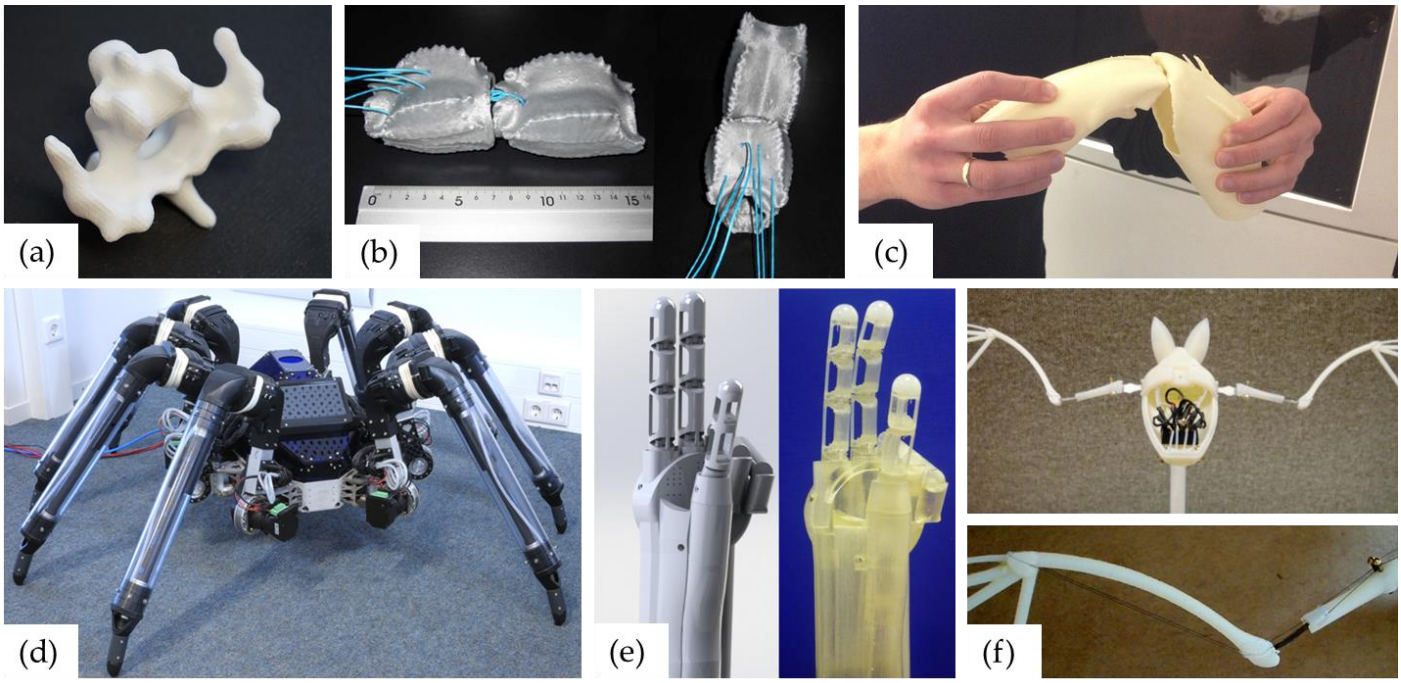


**Figure 1.** 3D printed analytical models of biological models are shown in the top row and technically converted, also 3D printed, joints are shown in the bottom row: (a) Owl cervical vertebra; (b) Scorpion tail joint [9]; (c) Spider leg joint [8]; (d) Bionic spider [8]; (e) Bionic hand [10]; (f) Bionic bat (BATMAV) with SMA actuator wires [11].

patterns can be applied to save material. Through these possibilities, bionic product development can be optimised in terms of quality, speed and, in particular, practical feasibility.

In combination with smart materials, in the here presented case wires made of shape memory alloys (SMA), the advantages mentioned come into their own. Actuators made of SMA generate their movement through a reversible phase transformation from martensite to austenite [10,11]. This phase transformation causes the actuator to remember a trained geometric shape, which gives it its name [12,13]. For example, it is possible to shorten a 100 mm long and 0.381 mm in diameter nickel-titanium (NiTi) wire by heating it to 70 - 100 °C to a length of about 95 mm and thereby lift a weight of 2000 g. The weight of the wire actuator is only 0.074 g (0.395 g with ring cable terminals) [14]. It is possible to make this muscle-like movement of the SMA wire actuators optimally usable for joint assemblies by means of AM carrier components. The problem of the difficult combination of high force, large stroke and small installation space can thus be addressed. The comparatively low stroke of the SMA wire actuators is often cited as the main difficulty of this actuation technology [15]. This problem can be tackled by appropriately fitting the SMA wire actuators in three-dimensional space. The highest energy density among the known actuator principles, which results in an enormous force with low self-weight, is the crucial factor [16,17]. A suitable mechanical transmission, which leads to a larger stroke with less force, can therefore be used.

The need to design such joint assemblies arose during research into a bionic joint robot arm (hyper redundant robot) based on the model of the cervical spine of American barn owls [18]. The delicate vertebral structures with the internal supply channels of the owl's neck [19] had to be technically abstracted and reproduced. In particular, the actuator selection and integration posed the greatest challenge. Only by using the aforementioned SMA wire actuators was it possible to implement the motions of the biological model of the barn owl within the framework of the tight installation spaces. The limitation of the use of the SMA wire actuators due to their small stroke was of less importance, as in the case of the owl's cervical spine many small movements of the individual cervical vertebrae produce a large overall movement. At the same time, the use of little raw material in AM

Preprints (www.preprints.org) | NOT PEER-REVIEWED | Posted: 22 February 2023 doi:10.20944/preprints202302.0388.v1

and SMA wire actuators made it possible to realise a resource-efficient arrangement of bionic joints.

The research presented here includes the combination of the bionically abstracted owl neck vertebrae, AM and smart materials actuators in the form of SMA wire actuators. More specifically, joint assemblies with different mechanical transmissions are presented. This joint assemblies were manufactured and examined by means of experiments. In the process, the prevailing disadvantage of SMA wire actuators in the form of the low stroke had to be compensated by the enormous potential of the highest energy density of SMA wire actuators [16,17] in combination with AM, so that generally applicable joint assemblies could be developed. The original idea for these joints was the cervical spine of the American barn owl with its 14 individual joints [19]. Based on the different joint assemblies, the potential of combining these topics is presented and made usable for other engineers and researchers in such a way that joint assemblies for the most diverse applications can be designed within a shortened development time. In particular, the focus is on the efficient use of resources through the material-saving potential of AM technology and SMA wire actuators [20]. This eliminates the use of conventional, heavy drives in the form of electric motors, hydraulics or pneumatics.

Figure 2 shows the development of the biologically inspired joints as a flow chart. The chronological representation clearly illustrates the entire development process, starting with the biological inspiration, through the biomechanical investigations and the motion simulation, to the first technical prototype and the resulting joints. In particular, the greatly reduced development process through the research presented in this article is illustrated on the right side of the figure. At the same time, the flow chart illustrates the structure of this paper.

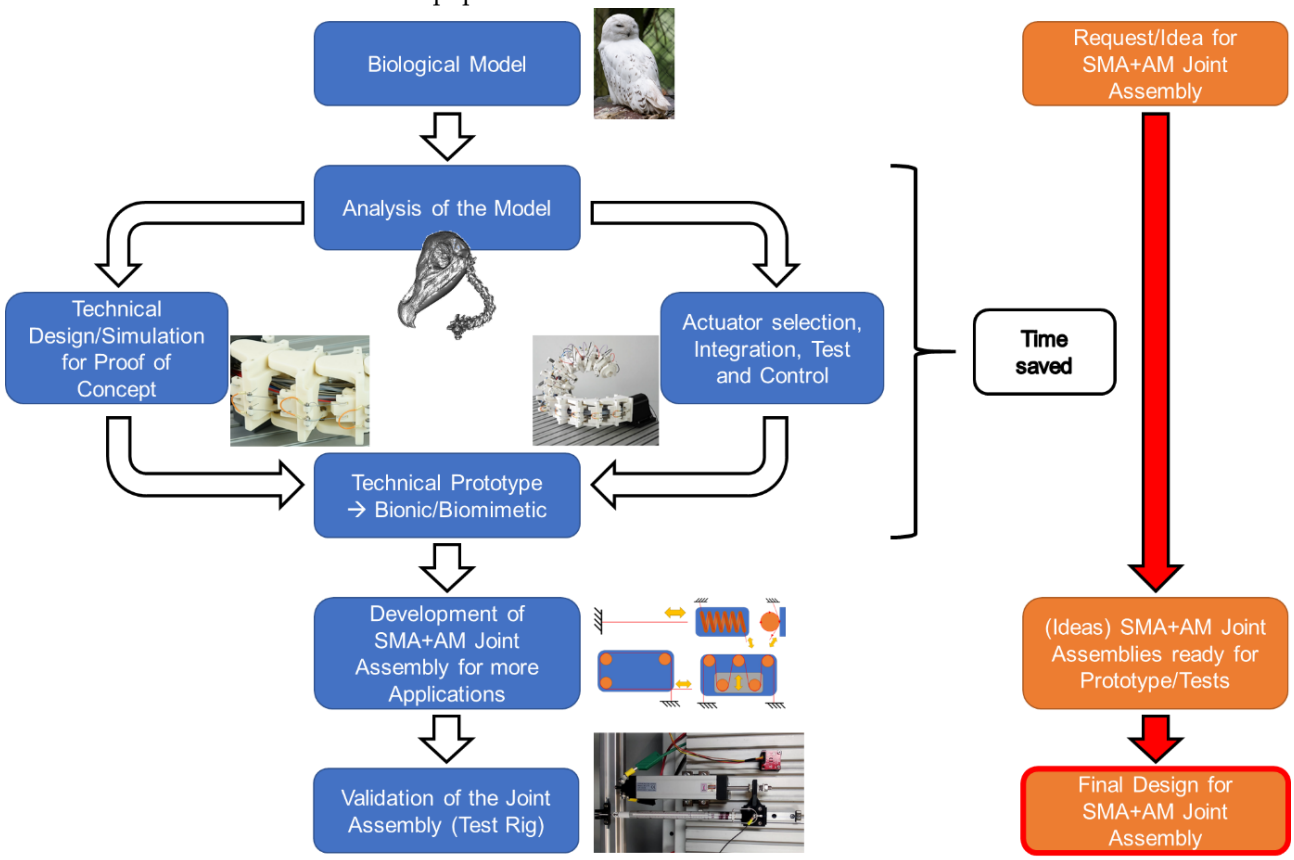


**Figure 2.** Flow chart illustrating the research process (left/blue) compared to the streamlined development process using the research results (right/orange).

Preprints (www.preprints.org) | NOT PEER-REVIEWED | Posted: 22 February 2023 doi:10.20944/preprints202302.0388.v1

## 2. Materials and Methods

### *2.1 Transfer of the Biological Model to Technical Joint Assemblies*

The necessary biological motion data as a foundation for the development of the joint assemblies could be obtained, evaluated and abstracted through the cooperation with the RWTH Aachen, Institute of Biology II (Zoology). There, the data was collected by analysing dissected American barn owls and X-ray as well as micro-CT images of the animals. The data was then further analysed in the form of 3D models. In this way, the great mobility of the cervical spine of American barn owls was proven and quantified. In particular, Krings et al. [21] described the subdivision of the cervical spine into three relevant areas of motion (see coloured areas in Figure 3). Depending on the range of motion, the individual movements of the cervical vertebrae take place around different axes of rotation. It was also found that saddle joints occur for the most part. Only the last two joints in the direction of the head differ from this. The second-last joint is a pivot joint. The last joint in front of the owl's head is a ball and socket joint. [19,21]

These data sets served as the basis for developing technically abstracted joint assemblies from the biological model of the individual joints. For this purpose, the slightly dif-

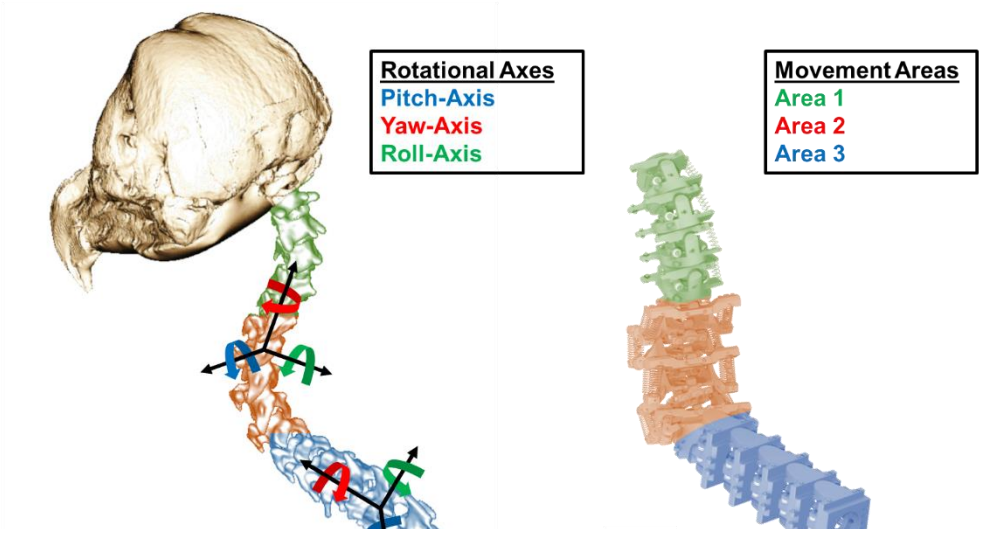


**Figure 3.** (a) Micro-CT image of the owl's neck spine with colour-coded rotational axes and movement areas; (b) Bionic model with analogue marked movement areas.

ferent articulation angles within the motion areas were adapted to each other so that only identical pairs of vertebrae were installed in each of the three motion areas. For example, this is clearly visible in the blue marked area 3 in Figure 3. Compared to the biological vertebrae on the left side, the technical vertebrae on the right side are exactly the same, which greatly simplified the production and following control concept. In addition, the saddle joints, which enable the movement of the respective pairs of vertebrae around two axes of rotation, have been reshaped into two successively linked rotary joints. This allowed a technical design in the form of a fixed bearing of the axes of rotation, whereby a doubling of the number of vertebrae took place. After the technical design of the cervical spine, its overall mobility was simulated and successfully verified with the help of inverse kinematics [22] in the development environment of Unity3D 2018.4.11f1 (Unity Technologies, San Francisco, US). The procedure for the simulative verification of the biological movement was described in [18] using a method developed specifically for this purpose.

### *2.2 Manufacturing of the Bionic and Technical Joints*

Different manufacturing processes were used to produce the bionic vertebrae of the robot arm and the technical joints of the test rig. The choice of process depended on the geometry and the mechanical as well as the thermal requirements of the parts. For example, milled components made of aluminium were selected for attaching measuring instruments to the test rig, as the force and stroke measurements would be affected by

Preprints (www.preprints.org) | NOT PEER-REVIEWED | Posted: 22 February 2023 doi:10.20944/preprints202302.0388.v1

deformed parts. The basic structure of the test rig was also made of aluminium profiles. Due to the robust setup, only the SMA wire and joint component deformations should influence the measurement. The actual bionic joint assembly parts were made of ABS-M30i using the FDM printing process on a Fortus 400mc Large (Stratasys Ltd., Rehovot, Israel). This was particularly beneficial for the prototype due to the free geometric design possibilities and the rapid manufacturing speed. The mechanical strength and temperature resistance of the components produced in this way are sufficient, taking into account the correct part orientation in the building chamber, because of the anisotropic mechanical properties [23]. The deflection components in contact with the SMA wire actuators were made of polytetrafluoroethylene (PTFE). This ensures mechanical stability even under temperatures up to 260 °C. Since the transformation temperatures of the SMA wires are 70 – 100 °C, PTFE is generally sufficient and recommended, as PTFE also insulates electrically. The PTFE components were manufactured conventionally, via turning or milling.

*2.3 Type of SMA Wire Actuators used*

SMA wire actuators (Dynalloy Inc., Irvine, US) were used to actuate the bionic joints in the prototype of the technical owl's neck and for the measurements in the test rig. More precisely, these were Flexinol Low Temperature (LT) wires, which are made of a NiTi alloy and have an activation temperature of approximately 70 °C. The Flexinol SMA wire actuators have the advantage that they are supplied ready for use and therefore additional training, as is the case with other commercially available wires, is not necessary [14]. Depending on the required pulling force, either 0.254 mm (0.01 in) or 0.381 mm (0.015 in) diameter wires were used in the bionic joint assemblies of the prototype. Wires with a diameter of 0.254 mm (0.01 in) were used in the test rig. The exact data of the SMA actuator wires can be found in Table 1 below.

**Table 1.** Application-related characteristics of the SMA wire actuators used [16]

| Characteristics | Flexinol LT 0.254 mm (0.01 in) | Flexinol LT 0.381 mm (0.015 in) |
|---|---|---|
| Resistance (Ω/m) | 18.5 | 8.3 |
| Maximum Pull Force (g) | 930 | 2000 |
| Approximate Contraction (%) | 4.5 | |
| Approximate Current at Room Temperature (mA) | 1000 | 2750 |
| Contraction Temperature (°C) | 70 | |
| Contraction Time (s) | 1 | 1 |
| Approximate cooling Time at 70 °C (s) | 5.5 | 13 |

According to the manufacturer, several tens of millions of cycles are possible if the values given in Table 1 are maintained. If the given operating temperature is exceeded, the number of cycles may be greatly reduced at first and the wire actuator may be damaged in the long run [14].

As shown in Figure 5, the SMA wire actuators were formed into loops at both ends and crimped with the help of ring cable terminals. This formed a force-fit connection between the SMA wire and the ring cable terminal. Fastening to the part was done by means of screw connections, which created a further frictional connection between the loop-shaped wire, the screw head and the contact surface of the ring cable terminal (see Figure 6 b and d). If the wire had slipped, this could be checked visually at the ring cable terminal. In the previous tests, no slippage could be observed. The crimping procedure is based on Czechowicz [10], the manufacturer's specifications [14] and VDI 2248 [20].

*2.4 Bionic Joint Assemblies*

Preprints (www.preprints.org) | NOT PEER-REVIEWED | Posted: 22 February 2023 doi:10.20944/preprints202302.0388.v1

Through the transfer described in chapter 2.1 from the biological model to technical joint assemblies, it was possible to develop a total of five bionic joint assemblies for the three cervical vertebrae areas as well as a gripper mechanism for the end effector. Of these six mechanisms in total, three joint assemblies were fundamentally different. These are shown as 3D models in Figure 4. The other three joint assemblies were analogously designed and are therefore not described separately. The information on the required wire lengths and forces resulted from geometric, weight and centre of gravity analyses of the CAD model. Appropriate safety factors were included for weight deviations of the physical prototype.

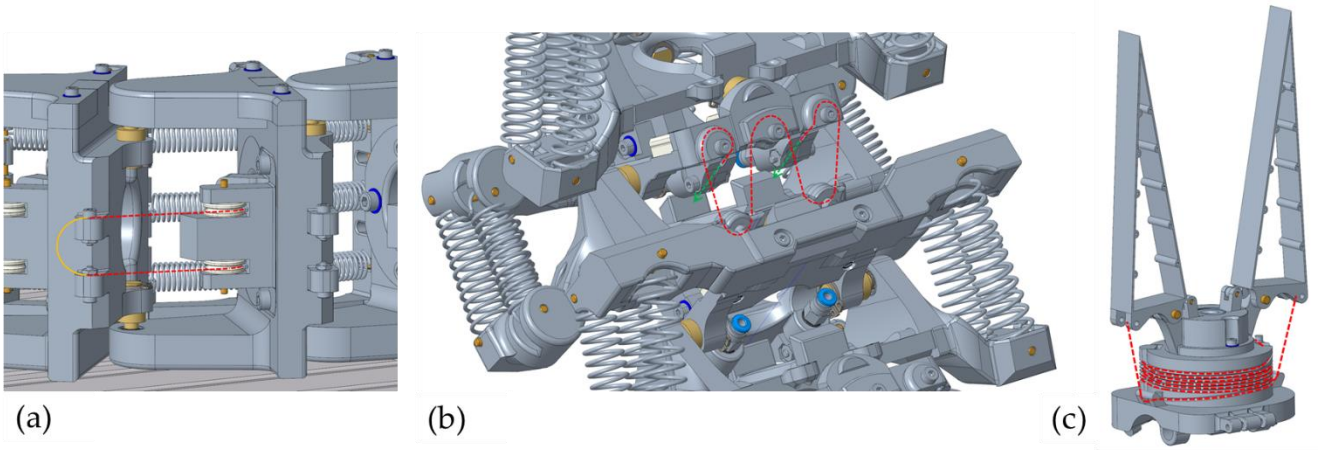


**Figure 4.** (a) Roll joint assemblies in the lower area; (b) Pitch joint assemblies in the middle area; (c) Finray gripper on the end effector; The SMA wire actuators are shown as red dashed lines.

2.4.1 Joint Assembly for the Roll Movement in the Lower Area (Area 3)

In Figure 4 (a), the joint assembly for generating the roll movement in the lower area of the owl's neck spine can be seen. Five of these were arranged successively, each of which generated ±22.5° as a single movement. This created a roll movement of ±112.5° in the entire area. As in the biological model, this resulted in a curved shape of area 3 of the cervical spine and the lateral offset of the following areas compared to the vertical centre axis [21]. The necessary force of theoretically 46.4 N was generated by the parallel installation of two SMA wire actuators with a diameter of 0.381 mm. The movement was reset by three parallel tension springs. In order to be able to provide the necessary wire length of the SMA actuators of 1500 mm for these joint assemblies, the wires were installed underneath the worktable and guided directly to the respective vertebrae by means of a bowden cable arrangement. The bowden cable consisted of the inner SMA wire, which is enclosed by a PTFE tube and a long tension spring. The bowden cable was mechanically connected by means of pneumatic connectors. As shown in Figure 4 (a) a pulley was attached to the vertebra for aligning the SMA wire, which guides the wire to the fastening screw of the following vertebra. For easier electrical wiring, the mechanically parallel FGL wires were electrically connected in series. This means that the positive and negative poles are located underneath the worktable.

2.4.2 Joint Assembly for Pitch Movement in the Middle Area (Area 2)

In Figure 4 (b), the second significantly different variant for installing the replacement muscles in the form of SMA wire actuators for producing the pitch movement of the middle section can be seen. Five joint assemblies were arranged in sequence for a possible total movement of ±125°. This movement is mainly for tilting and raising the end effector. It should be noted that a large negative movement resulted in a collision with the work table during this setup of the robot arm. Each of the individual joint assemblies generated a movement of ±25° and had to be able to move a force of 129.4 N in theory. To generate the force, an SMA wire with 0.381 mm was installed in each joint assembly in an arrangement comparable to a factor pulley. Due to the arrangement with four movable wires,

Preprints (www.preprints.org) | NOT PEER-REVIEWED | Posted: 22 February 2023 doi:10.20944/preprints202302.0388.v1

analogous to ropes in a pulley block, the load on the respective wire segments was reduced by a factor of four, whereby at the same time four times the wire length had to be installed to generate the movement of 23 mm. With a necessary safety factor, an SMA wire with a total length of approximately 2650 mm had to be installed. Analogous to the variant shown in Figure 4 (a), the SMA wires installed here were guided under the work table by means of bowden cables in order to install a greater wire length there. The difference here is that only one wire was installed per joint assembly. This was guided once upwards to the vertebra, installed there as shown and then guided back under the worktable. The wire was reset via parallel tension springs on both sides of the respective pair of vertebrae.

2.4.3 Joint Assembly for the Finray Gripper

The third variant can be seen in Figure 4 (c). This variant was used for the gripping movement of the finray gripper at the end effector. The basic function of the bionic finray gripper [24] is not part of this research project. In order to realise an energy-free holding position of the gripper, the gripping movement of the two jaws was realised with an internally installed tension spring. A 0.25 mm SMA wire actuator was used only for the quick opening movements of the gripper. This wire was wound spirally around the base body of the gripper in a 0.5 x 1 mm PTFE tube. This allowed a wire length of approximately 1000 mm to be fitted into the available installation space and a theoretical opening angle of 50° to be produced with sufficient holding force for a weight of 150 g. The use of a single SMA wire was sufficient for the assembly. This wire was attached with its two ends to the force engagement points of the gripper jaws. The electrical cables could be guided through the hollow inside of the gripper to the channel in the technical cervical spine. This resulted in a very compact mechanical and electrical design.

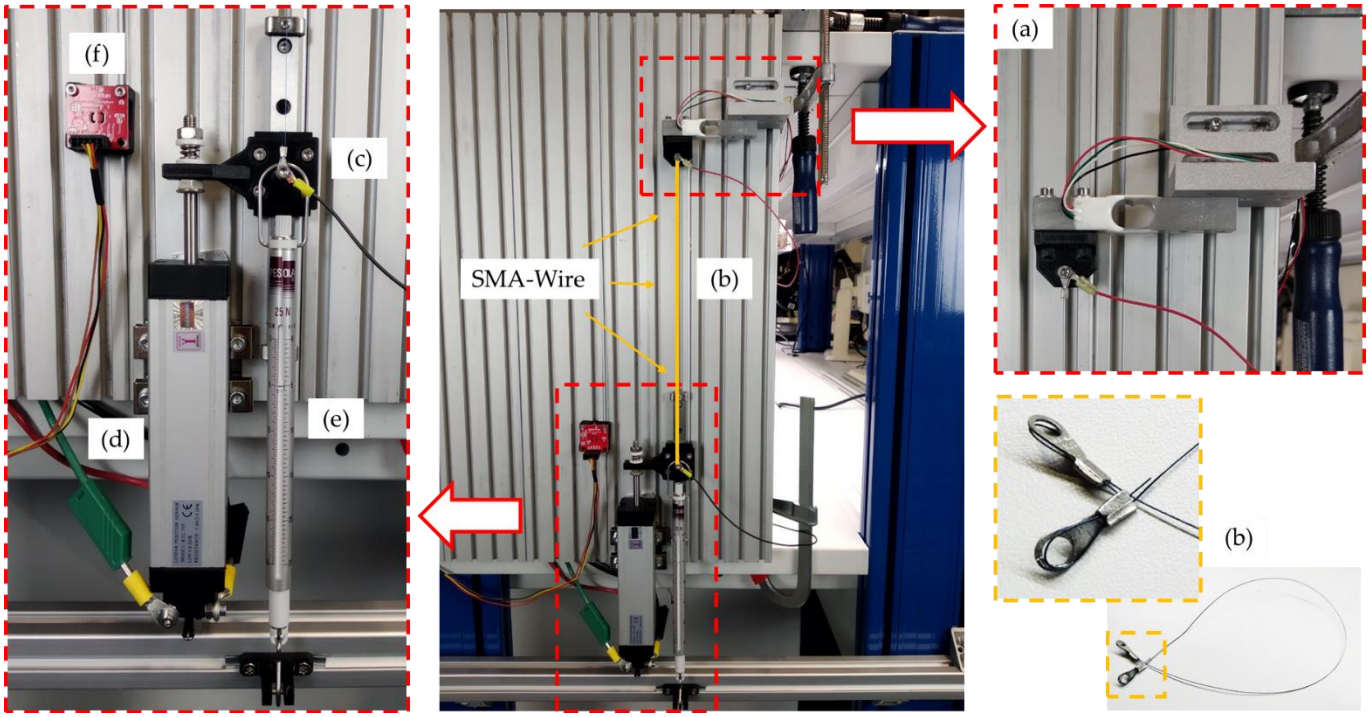


**Figure 5.** Vertical test rig for pre-tests: (a) Load cell Sauter CK 6-0P1 (KERN & SOHN GmbH, Balingen-Frommern, DE); (b) 250 x 0.25 mm SMA wire actuator; (c) Connecting platform; (d) Linear potentiometer KTC 75 P (Ixthus Instrumentation, Towcester, UK); (e) Tension spring balance Medio 25 N (PESOLA Präzisionswaagen AG, Schindellegi , CH) to generate the necessary counterforce; (f) Temperature sensor TMP117 (SparkFun Electronics, Boulder, US)

*2.5 Test Rig and Technical Joint Assemblies*

The bionic joint assemblies described in section 2.4 were further simplified, manufactured, installed in a specially developed test rig and analysed in pre-tests. Friction and

Preprints (www.preprints.org) | NOT PEER-REVIEWED | Posted: 22 February 2023 doi:10.20944/preprints202302.0388.v1

force losses in the deflection points as well as the general usability of the joint assemblies and the possibility of compact design were examined.

In the center of Figure 5, the vertically oriented mounting plate and the test rig assembly can be seen. Basically, the measurement setup always included a load cell at the upper end of the test rig (a), the SMA wire actuator clamped in between (b), a connecting platform between the SMA wire (c), the linear potentiometer (d) and a counterweight in the form of a tension spring balance at the lower end of the test rig (e). The arrangement of the SMA wire was variable due to different deflection variants. Thus, different wire lengths could be fitted and tested in different installation designs. Figure 6 shows a straight clamped SMA wire actuator as a reference measurement and three deflection variants, analogous to the vertebra assemblies in the bionic articulated robot arm described in section 2.4. The three deflection variants also include two sub-variants each. For all measurements, the 0.25 mm diameter SMA wires, described in section 2.3, were used in lengths of 250 mm, 450 mm and 750 mm. The PTFE pulleys shown were used in combination with ball bearings to minimize rolling friction. A detailed description of the deflection variants is shown in Table 2. In order to obtain repeatable results, a new SMA wire was used for each of the measurement series of the variants. All measurements were carried out at room temperature in the range of 21 – 24 °C.

As can be seen in Figure 7, the SMA wire was supplied with power at a constant voltage. The power was provided by a E36313A laboratory power supply unit (Keysight Technologies, Santa Rosa, US). The current results from the relationship between power and resistance. In the process of the current increase, a slight drop could be seen at about 0.6 A. This results, as described by Lewis et al. [25], from a short increase in resistance with increasing temperature. This causes the power and the temperature to drop for a short time. After less than four seconds, the current stabilised again and increased to the maximum. This behaviour results from the decreasing resistance as the phase

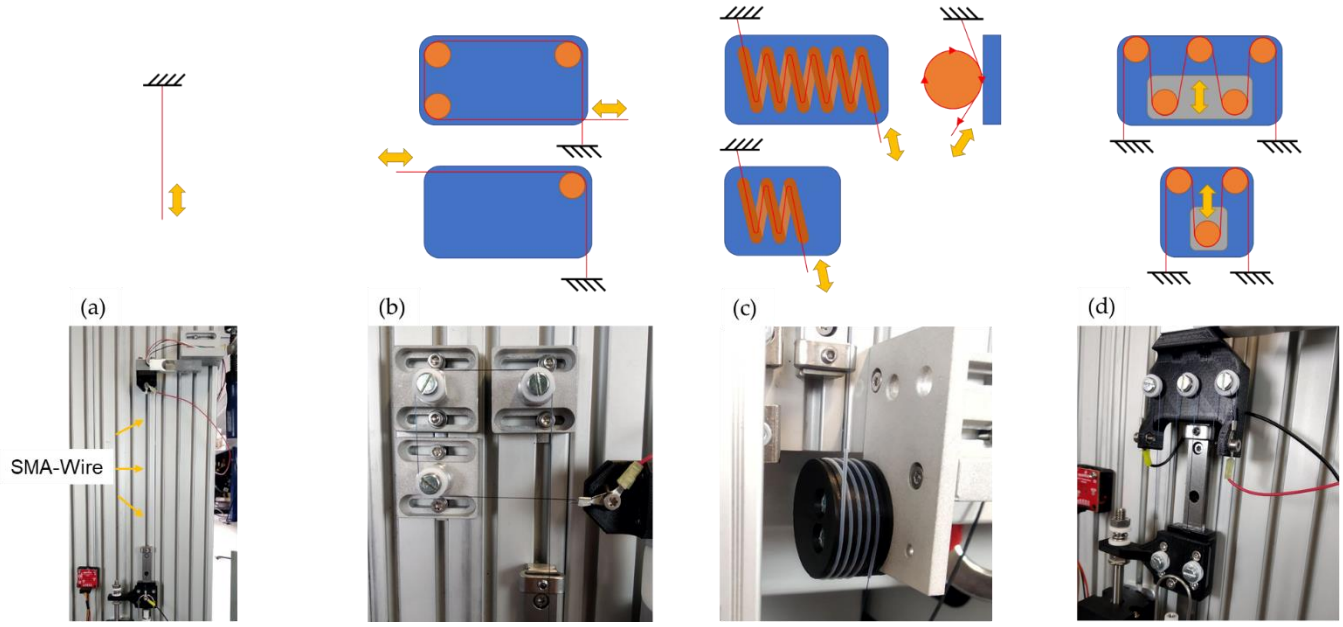


**Figure 6.** Different deflection variants in sketch are shown in the top row and final manufactured joint assemblies in the bottom row: (a) Straight clamped SMA wire for reference measurement; (b) Deflection variant using PTFE pulleys with 3 x 90° and 1 x 90° deflection; (c) Helix deflection in PTFE tube with Helix Short and Helix Long; (d) Pulley block with PTFE pulleys with Pulley Small and Pulley Big.

Preprints (www.preprints.org) | NOT PEER-REVIEWED | Posted: 22 February 2023 doi:10.20944/preprints202302.0388.v1

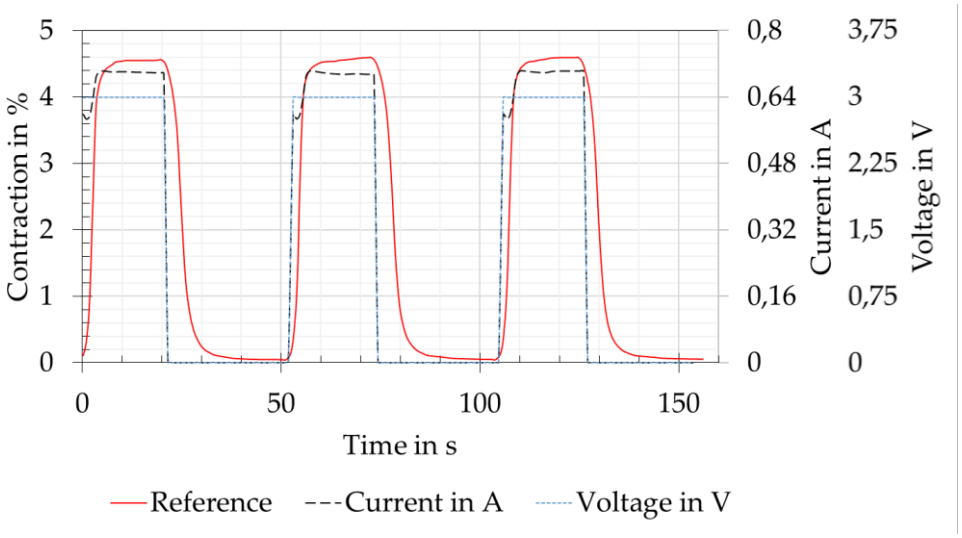


**Figure 7.** Relationship between the electric current, the voltage and the contraction of the SMA wire actuator on the basis of a reference measurement with a clamped straight wire. A constant voltage of 3 V was applied.

transformation and thus the contraction of the wire is continued. The geometric change therefore affects the resistance more than the temperature [26,27]. This behaviour could be seen in all test versions and could be tolerated for the pre-tests, as the maximum forces and contraction were reached within an acceptable time. For further tests, power control should be aimed for, as this can ensure a constant temperature during the phase transformation [25].

Data collection was done with a parallel system consisting of an Arduino Uno (Arduino, New York, US), a 34460A bench multimeter (Keysight Technologies, Santa Rosa, US) and an E36313A laboratory power supply unit (Keysight Technologies, Santa Rosa, US). The data from the Arduino Uno was collected with a self-developed software based on MATLAB (The MathWorks, Inc., Natick, US). The Keysight devices were operated and read out via BenchVue (Keysight Technologies, Santa Rosa, US). The evaluation is carried out with Microsoft Excel (Microsoft Corporation, Redmond, US).

**Table 2.** Description of the deflection versions and variants installed in the test rig. If there are several values per line, the values of the following line always refer to the order of the previous ones. If only one value is listed below, it applies to both previous values.

| Characteristics | Version Straight | Version Deflection | Version Helix | Version Pulley Block |
|---|---|---|---|---|
| Wire length (mm) | 250 | 250 | 750<br>450 | 450<br>250 |
| Wire guide (Variants) | / | 3 x 90°<br>1 x 90° | 4 x windings<br>2 x windings | 4 x movable wires<br>2 x movable wires |
| Guide material | / | Pulley (PTFE) | Tube (PTFE) | Pulley (PTFE) |
| Electrical current (A) | 0.7 | 0.7 | 1.1<br>0.9 | 0.7<br>0.7 |
| Electrical voltage (V) | 3 | 3 | 14<br>7 | 5.4<br>3 |
| Mechanical preload (N) | 5 | 5 | 5 | 10<br>5 |
| Time under power (s) | 20 | 20 | 20 | 20 |
| Cooling time (s) | 30 | 30 | 60<br>30 | 30 |

Preprints (www.preprints.org) | NOT PEER-REVIEWED | Posted: 22 February 2023 doi:10.20944/preprints202302.0388.v1

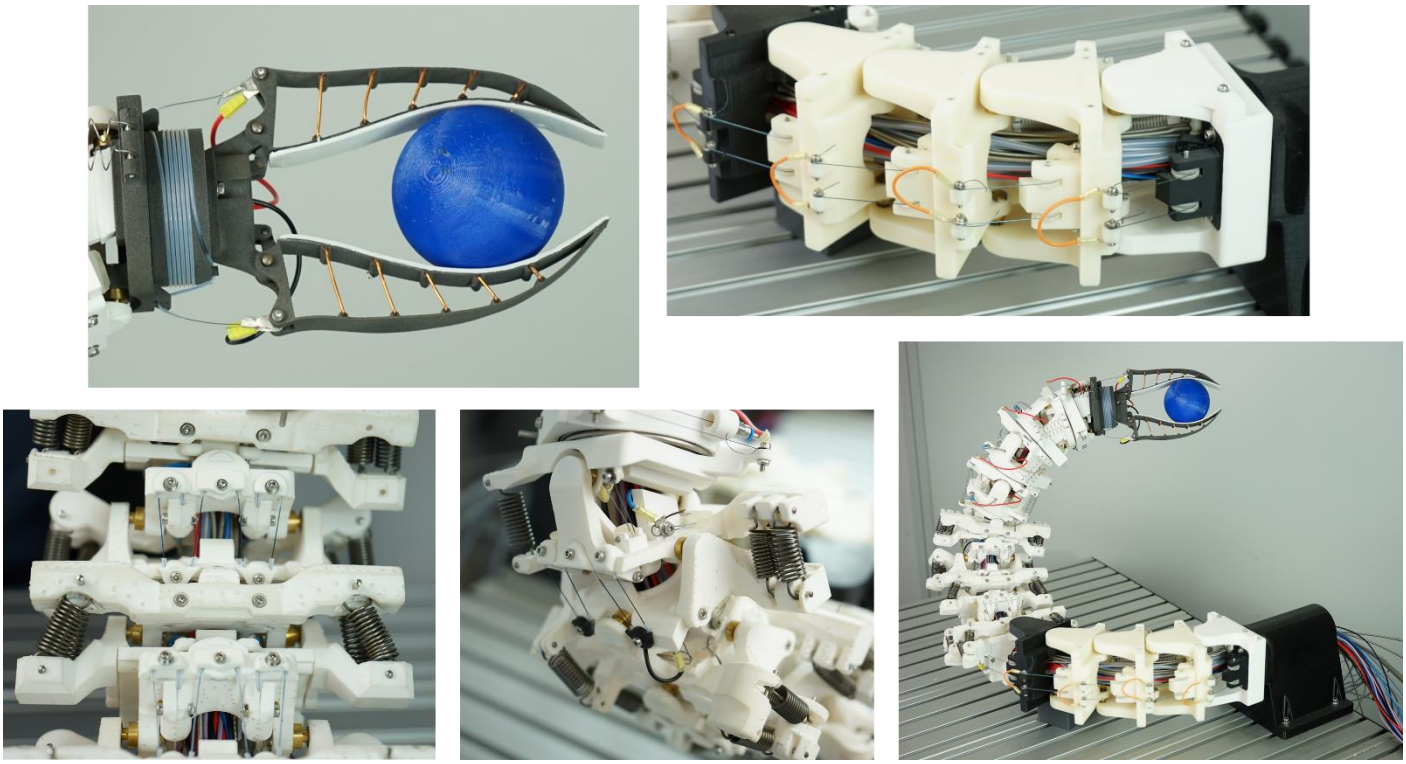

**Figure 8.** Prototype of the bionic owl neck spine and fundamentally different joint assemblies.

## 3. Results and Discussion

*3.1 Bionic Joint Assemblies of the Owl's Neck Spine*

In the developed prototype (Figure 8), the SMA wire actuators described in chapter 2.3 with diameters of 0.25 mm and 0.381 mm were built into the bionic vertebrae of the articulated robot arm described in chapter 2.4 and manufactured using the AM manufacturing technologies of chapter 2.2.

With the prototype shown, the requirements of the VDI guideline 6220 [28], which are needed for a bionic system, were fulfilled as listed below. The description of the successfully developed prototype using this guideline is done for general illustration and possible comparison with other bionic systems. The discussion of the current prototype follows after chapter 3.1.3.

3.1.1 A Biological Model is available

As described in section 2.1, the model of the highly flexible owl neck spine of American barn owls was available. The biologically possible movements and joint arrangements were described in detail by Krings et al. [19,21] and were used as the foundation for the articulated robot arm shown in Figure 8. Approximately, the biological model had a possible head rotation of 270° around the vertical axis and 180° around the horizontal axis [21].

3.1.2 The Working Principle is abstracted and transferred into a Technical Application

Abstracted technical cervical vertebrae were available for the design of an articulated robotic arm modelled on the owl's cervical spine. The 14 biological cervical vertebrae, which were lined up and primarily linked with saddle joints, consisted of 23 rotary joints in the technical version. In all cases, the rotary joints consisted of brass shafts and ball bearings. This design was chosen due to the lack of technical saddle joints. As muscle substitutes, SMA wire actuators were installed as agonist and different tension springs as antagonist. Simulation results in the form of reachability maps [18] were available to simulate the theoretical range of motion. In addition, the supply channels found in biology in the centre of the vertebrae were technically replicated and used to install the electrical supply lines and the SMA wire actuators.

Preprints (www.preprints.org) | NOT PEER-REVIEWED | Posted: 22 February 2023 doi:10.20944/preprints202302.0388.v1

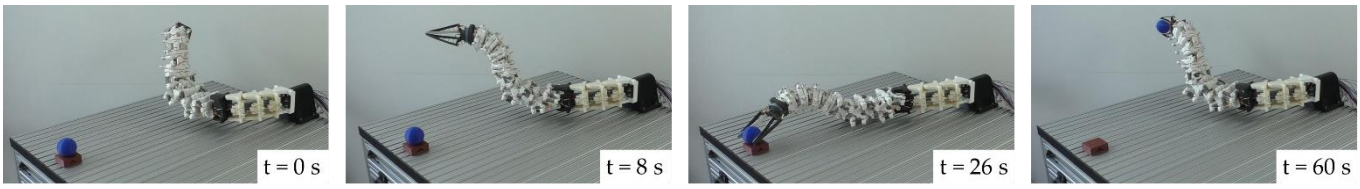


**Figure 9.** Movement sequence for pivoting, tilting and gripping a sphere. The duration of the entire sequence was 60 seconds.

3.1.3 A Prototype of the Implementation is available

Due to the described abstracted working principle of the individual joint assemblies and the simulation of the range of motion to control the prototype, the natural motions of the owl's neck spine could be executed. Movements could be performed over almost the entire working area of 900 x 800 mm and objects with different geometries could be grasped. Figure 9 shows in four pictures an exemplary movement sequence for picking up a spherical object. In this movement, the use of the three significantly different joint assemblies, namely the roll movement in the lower area, the pitch movement in the middle area and the gripping movement, can be seen very clearly. These three bionic joint assemblies served as models for the technically abstracted joint assemblies in the test rig. In addition to this, another main movement was performed for the rotation of the finray gripper by the yaw movement in the upper area of the articulated robot arm.

Compared to existing hyper redundant and continuum robots, the muscle-like drives in the form of SMA wire actuators stood out. Other systems used, for example, cable-driven systems with conventional electrical motors [29,30]. In this case, the cables had to be routed through the inside of the robot arm, analogous to the bowden cables of the bionic owl's neck spine. This resulted in a massive base body to which the corresponding motors for the cable were attached. Another drive option was the direct use of electric motors, which were installed directly in the robot arm. This can be demonstrated using the example of snake robots, which are also classified as hyper redundant robots due to their large number of joints [31]. The weight of the directly mounted motors had to be moved as well. Another comparable robot arm is the continuum robot by Mahl et al. [32] which was pneumatically driven and was based on the biological model of the elephant trunk. This system is characterised by its inherent compliance. However, an external pneumatic unit was needed to generate movement. Compared to the aforementioned robotic arms, the bionic owl neck spine had an extremely light dead weight of the drives. However, the weight was increased by the bowden cables used and by the deflections under the work table. Overall the low material input of the NiTi alloys of the SMA wire actuators used less critical materials than, for example, rare earths in electric motors. This and the lightweight AM components fulfilled the requirement of a resource-efficient system. The disadvantage of this actuator technology was the slow movements of the robot arm. This was caused by the necessary cooling times of the SMA wires, which were further increased by the bowden cables. The movement in Figure 9, for example, took 60 seconds.

*3.2 Technical Joint Assemblies and Experimental Results*

In the following, the experimental results of the technical joint assemblies from chapter 2.5 are described and evaluated. The experiments were carried out with the components and parameters listed in Table 2. An important influence in the coupled force and displacement measurements was the tension spring balance used. Due to the linear spring constant of 0.25 N/mm, a higher force always occurred with increasing shortening of the SMA wire actuator. An experimental setup with a longer integrated wire and thus a greater absolute shortening therefore resulted in a higher measured force.

Preprints (www.preprints.org) | NOT PEER-REVIEWED | Posted: 22 February 2023 doi:10.20944/preprints202302.0388.v1

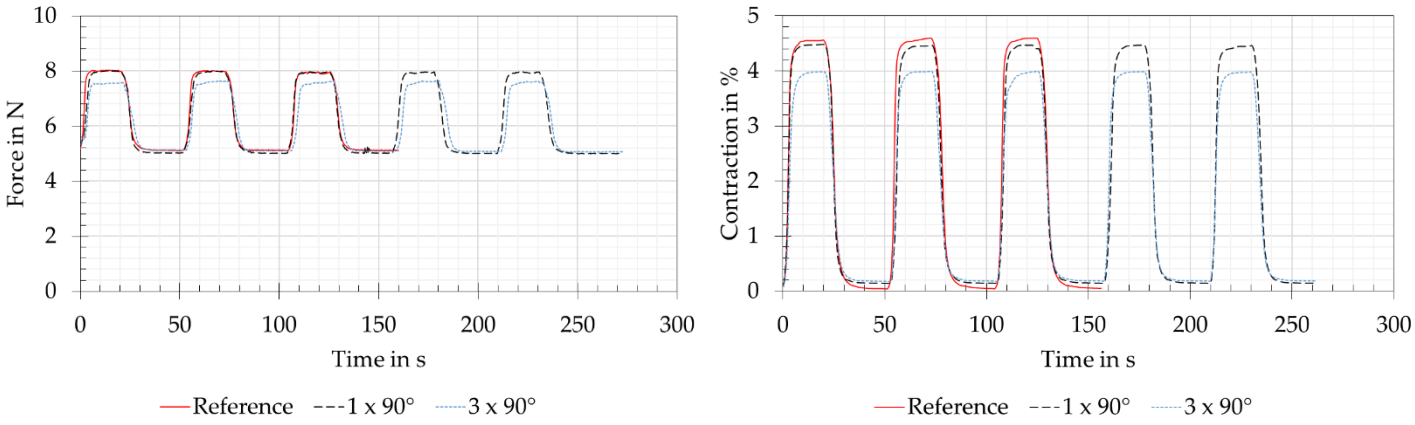


**Figure 10.** Versions Straight and Deflection: Force and contraction measurements for the reference measurement on the straight clamped SMA wire actuator, the deflection by 1 x 90° and 3 x 90°. The wire length was 250 mm for all deflection versions, measurements are taken with 5 N.

3.2.1 Version Straight

The force and contraction measurements of version Straight are shown as red lines in Figure 10. This version was the reference measurement with a straight piece of wire clamped, without deflection. The set preloading force of 5 N and the force of 7.9 N, which could be read off the tension spring balance at the specified power, are shown with slight deviations on the left-hand side of Figure 10. The measurement of the wire contraction is shown on the right side of Figure 10 and was approximately 4.6 % for a full phase transformation of the SMA. The assumption for full phase transformation refers to the plateaus seen when maximum force and contraction were reached. The wire contraction matched the manufacturer's data from Table 1 [14]. The measurements also appeared plausible due to the mathematically correct measured force difference of 2.875 N at a shortening of 4.6 % (11.5 mm) with a spring constant of 0.25 N/mm of the tension spring balance. After each run, the SMA wire actuator also returned to its initial shape at 0 % shortening and 5 N preloading force.

3.2.2 Version Deflection

The force and displacement measurements of the joint variants of version Deflection are shown in Figure 10 for direct reference with version Straight. This is due to the fact that the wire lengths and electrical power ratings were the same (see also Table 2). The force measurements yielded almost identical results to the reference for the variant with "1 x 90°" deflection and the measured force decreases by 0.4 N for the variant "3 x 90°". The contraction measurements of the "1 x 90°" and "3 x 90°" variants showed losses of 0.1 % and 0.6 %. At the same time, a small remaining contraction of 0.1 - 0.2 % remained with both variants. As with version Straight, plateaus appeared in the contraction measurement in the powered state, from which a completed phase transformation of the wire actuators could be concluded. The force and contraction losses resulted from friction and temperature losses in the deflection points and therefore increased with an increasing number of deflection pulleys. The loss of contraction due to the use of pulleys was also observed in fatigue tests by Mohd Jani [15]. It can be expected that the force and contraction values of the reference measurement can be achieved with a higher electrical power and thus a higher energy consumption.

3.2.3 Version Helix

The force and contraction measurements of the joint variants of version Helix are shown in Figure 11. It should be noticed that the cooling time of the Helix Long version had been doubled from 30 to 60 seconds and that the electrical performance data had been increased by factors of 1.66 (Helix Short) and 2.44 (Helix Long). In the force measurements

Preprints (www.preprints.org) | NOT PEER-REVIEWED | Posted: 22 February 2023 doi:10.20944/preprints202302.0388.v1

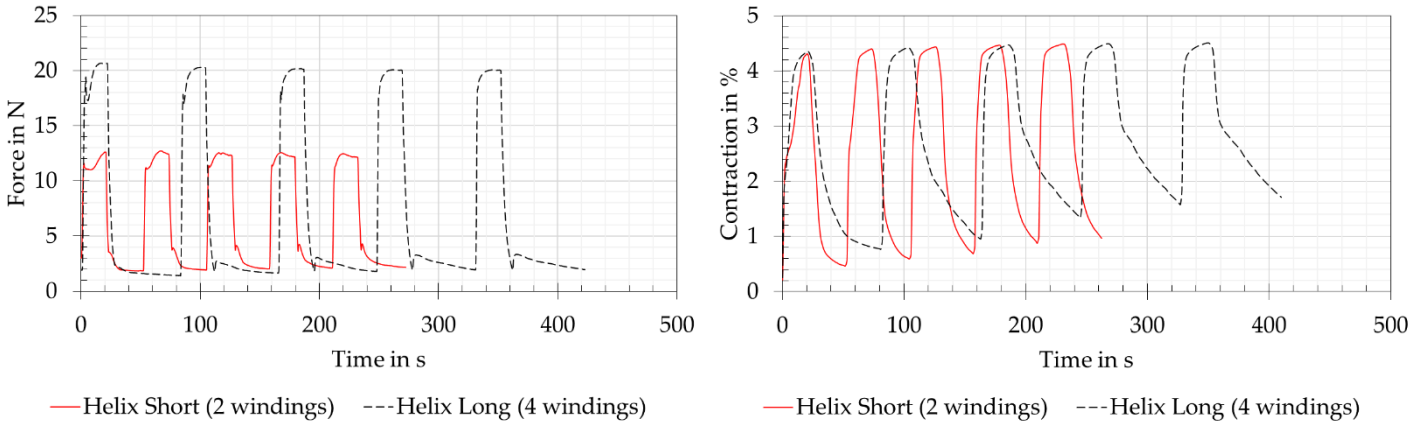


**Figure 11.** Version Helix: Force and contraction measurements for the Helix Short and Helix Long variants. The wire length was 450 mm for Helix Short and 750 mm for Helix Long. The Helix Short was supplied with 7 V and 0.9 A and the Helix Long with 14 V and 1.1 A. Both versions were preloaded with 5 N.

of the Helix Short and Helix Long variants, no direct comparison could be made with the reference measurement of version Straight due to the mechanically very different design and the different wire lengths of 450 mm and 750 mm. However, it was possible to compare the values measured with the load cell with the analogue force display values of the tension spring balance. When supplied with power, the force displayed on the tension spring balance was 9.7 N for the Helix Short variant and 12.5 N for the Helix Long variant. In both variants, a strongly increased force was measured at the load cell, which was due to strong friction losses within the SMA wires with PTFE tubing wrapped helically around a base body. When the measured force increased, both variants initially had a peak which dropped again and then rised to the final force value. This can be explained by the inhomogeneous and thus time-delayed shortening of the air exposed wire sections or those covered by the PTFE tube and by the friction within the tube. It can be assumed that the exposed section of the SMA-wire attached to the load cell first contracted and at the same time, due to the friction within the tube, could only pull the tension spring balance with a high degree of friction. The open wire section underneath the tube contracted at the same time, but had little influence on the load cell's force measurement. After a short time, the SMA wire in the tube was also heated up and the full contraction could be measured, but with increased force measurement due to the friction within the tube system. This assumption was confirmed for both variants, as the tube systems were heated up with increasing measurement cycle repetitions and the effect therefore no longer occurred in the fifth measurement cycle. The measured contractions of the two variants showed almost 4.5 %, which corresponded to the reference measurement. This is contrary to the experimental results of [33]. There, a loss of 35 % of the contraction is given when the wire is wound 360°. This may be due to the higher force of 100 N for a wire diameter of 0.7 mm. However, the contraction of 4,5 % in the design shown here could only be achieved by the increased electrical power mentioned at the beginning of this chapter, as the tube system in combination with the base body acted as a large heat sink for the SMA wire. This observation and a general heating of the system is confirmed by the measurements of [33]. This resulted in a loss of dynamic performance of the actuator system. At the same time, an increase in maximum contraction and a not complete relaxation of the wires could be observed with an increasing number of cycles. This could be explained by the heating of the tube system. In general, this design made it possible to fit a larger contraction into a more compact installation space. This is confirmed by the test results of Helps et al. [34], which show an increased shortening of 69.81 % in the same installation space compared to a straight wire.

Preprints (www.preprints.org) | NOT PEER-REVIEWED | Posted: 22 February 2023 doi:10.20944/preprints202302.0388.v1

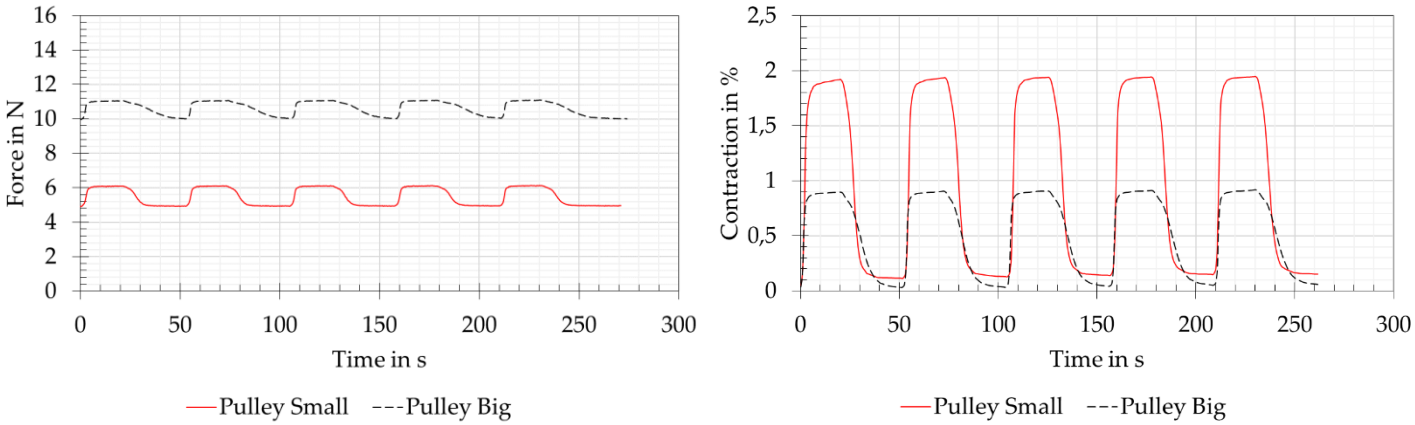


**Figure 12.** Version Pulley Block: Force and contraction measurements for the Pulley Small and Pulley Big variants. The wire length was 250 mm for the Pulley Small and 450 mm for the Pulley Big. The Pulley Small was supplied with 3 V and 0.7 A and was preloaded with 5 N. The Pulley Big was supplied with 5.4 V and 0.7 A and preloaded with 10 N.

3.2.4 Version Pulley Block

The force and contraction measurements of the joint variants of version Pulley Block are shown in Figure 12. These two variants were supplied with electrical power in the matching factor, related to the wire lengths, for the reference measurement. It should be noticed that a doubled preload force of 10 N was used for the Pulley Big variant, as otherwise a total reset of the system to the preload force of 5 N was not achievable. For the Pulley Small variant, the preload force remained at 5 N, analogous to the reference measurement. The forces that could be read off the tension spring balance when powered are 6.1 N for Pulley Small and 11 N for Pulley Big. Both force measurements were carried out with the load cell showing very similar results and therefore seemed plausible. The small differences in force between the preload force and the maximum force resulted from the pulley arrangement, whereby the contraction of the system decreased as a factor of the number of moving wires. This could be clearly seen in the contraction measurements. In combination with friction losses due to the multiple consecutive 180° deflections of the SMA wire, analogous to version Deflection, the pulley arrangement resulted in the relatively represented contraction of the system in a factor of two for Pulley Small and four for Pulley Big. Due to the mostly air exposed SMA wires, the heating and cooling time was little influenced by the deflection pulleys. The use of such pulleys to increase the force in the SMA system is recommended by [15] and applied by [35] to develop a vacuum gripper. This vacuum gripper works with a tension spring to generate the vacuum and with the SMA wires arranged in a circle like pulley system to generate the necessary reset force. Based on the own test results and the described successful applications of other researchers, this pulley variant can be used for joint variants with high force requirements at low contraction.

## 5. Conclusions and Outlook

This article presents the development of additively manufactured joint assemblies with SMA wire actuators as drive technology. Additive manufacturing is mainly characterised by the possibility of geometrically flexible design. The SMA wire actuators offer the highest energy density among the known actuator technologies [16,17]. With the combination of these potentials, it was possible to integrate large wire lengths into compact joint assemblies and thus develop actuator assemblies with large strokes, acceptable forces and high resource efficiency. The basic design ideas for the joints originated from a bionics project to develop an articulated robot arm modelled on the American barn owl. This involved working on the problem of fitting large SMA wire lengths into compact bionic owl neck vertebrae.

Using an additively manufactured prototype of the bionic owl's neck spine with integrated SMA wire actuators as muscle substitutes, the basic function of the flexible movement could be reproduced. The 14 biological cervical vertebrae, most of which occur as saddle joints, were abstracted as 28 technical rotary joints and finally realised as 23 rotary joints.

With the demonstrated function of the bionic owl's neck as a basis, further abstracted technical joints were developed and their basic function and basic performance data (force and contraction) were first examined with the help of a test rig within the framework of preliminary tests. The basic function of all technical joints could thus be proven. This made it possible to integrate longer wire lengths of SMA actuators into more compact design volumes. It should be noted that a larger number of deflection points or windings resulted in increased force and contraction losses. In addition, it is known from research results [15,36] that material fatigue and thus a shortened lifetime can be expected.

The test rig used will be upgraded in the form of a frictionless bearing and a non-contact displacement measurement system in order to be able to continue the development of the joint assemblies. This is intended to further quantify the measurements described in this article in order to optimise friction and temperature losses in the deflection points. In addition, the joint assemblies will be further developed with regard to lightweight design and the resulting resource efficiency, e.g. through topology-optimised AM carrier components, and the use of further AM manufacturing technologies, e.g. SLM. In addition, the findings of the measurements carried out on the joint assemblies will be made available to other researchers and engineers within the framework of a design guideline with design catalogues. This should enable shorter and thus more efficient development processes for innovative SMA+AM joint assemblies.

**Author Contributions:** Conceptualization, R.L.; methodology, R.L.; software, R.L.; validation, R.L., S.T. and R.H.; formal analysis, R.L.; investigation, R.L.; resources, R.H.; data curation, R.H.; writing—original draft preparation, R.L.; writing—review and editing, S.T. and R.H.; visualization, R.L.; supervision, S.T. and R.H.; project administration, S.T. and R.H.; funding acquisition, R.H. All authors have read and agreed to the published version of the manuscript.

**Funding:** This research was funded by the Bavarian State Ministry of the Environment and Consumer Protection within the project network BayBionik (Project P8 An Owl-Neck Joint for more Efficient Machines, TUT01UT-73845).

**Data Availability Statement:** Further information and video on the bionics project of the technical owl's neck spine can be found under the following links:
https://baybionik.de/teilprojekte/p8-eulenhalsgelenk/ (accessed on 12 December 2022)
https://www.youtube.com/watch?v=3Cl38fQV76g (accessed on 12 December 2022)

**Acknowledgments:** R.L. und R.H. thank the coordination office of BayBionik project network very much for frequent network meetings, which allowed a fruitful knowledge exchange on bionics, sustainability and resource conservation.
H. Wagner and M. Krings from Institute of Biology II (Zoology) at RWTH Aachen University, Germany are thanked very much for cooperation in terms of biological data.
R.L. and R.H. greatly acknowledge the continuous support of Nuremberg Institute of Technology, Germany.
R.L. and S.T. also greatly acknowledge the continuous support of University of Bayreuth, Germany.

**Conflicts of Interest:** The authors declare no conflict of interest. The funders had no role in the design of the study; in the collection, analyses, or interpretation of data; in the writing of the manuscript, or in the decision to publish the results.

**References**


1. Rost, A.; Schadle, S. The SLS-Generated Soft Robotic Hand - An Integrated Approach Using Additive Manufacturing and Reinforcement Learning. In *2013 12th International Conference on Machine Learning and Applications.* 2013 12th International Conference on Machine Learning and Applications (ICMLA), Miami, FL, USA, 04–07 Dec. 2013; IEEE, 2013 - 2013; pp 215–220, ISBN 978-0-7695-5144-9.
2. Mohammed, I.H.; Gallardo, N.; Benavidez, P.; Jamshidi, M.; Champion, B. Design and control architecture of a 3D printed modular snake robot. In *2016 World Automation Congress (WAC).* 2016 World Automation Congress (WAC), Rio Grande, PR, USA, 31 Jul.–04 Aug. 2016; IEEE, 2016 - 2016; pp 1–6, ISBN 978-1-8893-3551-3.
3. Davis, S.; Tsagarakis, N.G.; Caldwell, D.G. The initial design and manufacturing process of a low cost hand for the robot iCub. In *Humanoids 2008 - 8th IEEE-RAS International Conference on Humanoid Robots.* Humanoids 2008 - 8th IEEE-RAS International Conference on Humanoid Robots, Daejeon, Korea (South), 01–03 Dec. 2008; IEEE, 2008 - 2008; pp 40–45, ISBN 978-1-4244-2821-2.
4. S. Jung; J. Bae; I. Moon. Lightweight prosthetic hand with five fingers using SMA actuator. *11th International Conference on Control, Automation and Systems* **2011**.
5. Zäh, M. *Wirtschaftliche Fertigung mit Rapid-Technologien*: *Anwender-Leitfaden zur Auswahl geeigneter Verfahren;* Hanser: München, Wien, 2006, ISBN 978-3-446-43957-3.
6. Landkammer, S. Grundsatzuntersuchungen, mathematische Modellierung und Ableitung einer Auslegungsrichtlinie für Gelenkantriebe nach dem Spinnenbeinprinzip; FAU University Press, 2019.
7. Günther, A.; Drack, M.; Monod, L.; Wirkner, C.S. A unique yet technically simple type of joint allows for the high mobility of scorpion tails. *J. R. Soc. Interface* **2021**, *18*, 20210388, doi:10.1098/rsif.2021.0388.
8. Simone, F.; Rizzello, G.; Seelecke, S. Metal muscles and nerves—a self-sensing SMA-actuated hand concept. *Smart Mater. Struct.* **2017**, *26*, 95007, doi:10.1088/1361-665X/aa7ad5.
9. Bunget, G.; Seelecke, S. BATMAV: a 2-DOF bio-inspired flapping flight platform. In *Active and Passive Smart Structures and Integrated Systems 2010.* SPIE Smart Structures and Materials + Nondestructive Evaluation and Health Monitoring, San Diego, California, USA, Sunday 7 March 2010; Ghasemi-Nejhad, M.N., Ed.; SPIE, 2010; 76433B.
10. Langbein, S.; Czechowicz, A. *Formgedächtnistechnik*: *Entwickeln, Testen und Anwenden*, 2., überarb. u. erw. Auflage 2021; Springer Fachmedien Wiesbaden: Wiesbaden, 2021, ISBN 9783658179045.
11. *Adaptronics and Smart Structures*: *Basics, Materials, Design, and Applications;* Janocha, H., Ed., 2. 2nd, rev. ed. 2007; Springer Berlin Heidelberg: Berlin, Heidelberg, 2007, ISBN 9783540719670.
12. Chang, L.C.; Read, T.A. Plastic Deformation and Diffusionless Phase Changes in Metals — the Gold-Cadmium Beta Phase. *JOM* **1951**, *3*, 47–52, doi:10.1007/BF03398954.
13. Chang, L. *Atomic Displacements and crystallographic mechanism in diffusionless transformation of gold-cadmium crystals containing 47.5 atomic percent cadmium*; Columbia Univ NYO-756. Available online: https://www.osti.gov/biblio/4422776.
14. Dynalloy Inc. Technical Characteristics of Flexinol Actuator Wires. Available online: http://www.dynalloy.com/pdfs/TCF1140.pdf (accessed on 6 December 2022).
15. J Mohd Jani. *Design optimisation of shape memory alloy linear actuator applications*, 2016.
16. Kohl, M. *Entwicklung von Mikroaktoren aus Formgedächtnislegierungen*, 2002.
17. Fumagalli, L.; Butera, F.; Coda, A. SmartFlex® NiTi Wires for Shape Memory Actuators. *J. of Materi Eng and Perform* **2009**, *18*, 691–695, doi:10.1007/s11665-009-9407-9.
18. Löffler, R.; Rücker, D.; Müller, F.; Hornfeck, R. Method for simulative reproduction, verification and technical adaptation as part of biological kinematics studies. *Procedia CIRP* **2021**, *100*, 649–654, doi:10.1016/j.procir.2021.05.138.

19. Krings, M.; Nyakatura, J.A.; Fischer, M.S.; Wagner, H. The cervical spine of the American barn owl (Tyto furcata pratincola): I. Anatomy of the vertebrae and regionalization in their S-shaped arrangement. *PLoS One* **2014**, *9*, e91653, doi:10.1371/journal.pone.0091653.
20. Verein Deutscher Ingenieure. *VDI 2248 Product development using shape memory alloys (SMA)*: *Basics and application examples*, 2019, *77.100, 77.120.99*.
21. Krings, M.; Nyakatura, J.A.; Boumans, M.L.L.M.; Fischer, M.S.; Wagner, H. Barn owls maximize head rotations by a combination of yawing and rolling in functionally diverse regions of the neck. *J. Anat.* **2017**, *231*, 12–22, doi:10.1111/joa.12616.
22. Starke, S.; Hendrich, N.; Zhang, J. Memetic Evolution for Generic Full-Body Inverse Kinematics in Robotics and Animation. *IEEE Trans. Evol. Computat.* **2019**, *23*, 406–420, doi:10.1109/TEVC.2018.2867601.
23. Stratasys Ltd. ABS-M30i product data sheet. Available online: https://www.stratasys.com/siteassets/materials/materials-catalog/fdm-materials/abs-m30i/mds_fdm_absm30i_0621a.pdf?v=48ded0 (accessed on 16 December 2022).
24. Leif Kniese. Load carrying element with flexible outer skin Abstract. 00250109.6, April 1, 2000.
25. Lewis, N.; York, A.; Seelecke, S. Experimental characterization of self-sensing SMA actuators under controlled convective cooling. *Smart Mater. Struct.* **2013**, *22*, 94012, doi:10.1088/0964-1726/22/9/094012.
26. Paul Motzki. Advanced Design and Control Concepts for Actuators Based on Shape Memory Alloy Wires; Universität des Saarlandes, Saarbrücken, 2018.
27. Schiedeck, F. *Entwicklung eines Modells für Formgedächtnisaktoren im geregelten dynamischen Betrieb*. Zugl.: Hannover, Univ., Diss., 2009; PZH Produktionstechn. Zentrum: Garbsen, 2009, ISBN 978-3-941416-23-9.
28. Verein Deutscher Ingenieure. *VDI 6220 Biomimetics Fundamentals, conception, and strategy*, 2021, *07.080* (accessed on 9 December 2022).
29. Martín-Barrio, A.; Roldán-Gómez, J.J.; Rodríguez, I.; Del Cerro, J.; Barrientos, A. Design of a Hyper-Redundant Robot and Teleoperation Using Mixed Reality for Inspection Tasks. *Sensors (Basel)* **2020**, *20*, doi:10.3390/s20082181.
30. Tang, L.; Wang, J.; Zheng, Y.; Gu, G.; Zhu, L.; Zhu, X. Design of a cable-driven hyper-redundant robot with experimental validation. *International Journal of Advanced Robotic Systems* **2017**, *14*, 172988141773445, doi:10.1177/1729881417734458.
31. Wright, C.; Johnson, A.; Peck, A.; McCord, Z.; Naaktgeboren, A.; Gianfortoni, P.; Gonzalez-Rivero, M.; Hatton, R.; Choset, H. Design of a modular snake robot. In *2007 IEEE/RSJ International Conference on Intelligent Robots and Systems*. 2007 IEEE/RSJ International Conference on Intelligent Robots and Systems, San Diego, CA, USA, 29 Oct.–02 Nov. 2007; IEEE, 2007 - 2007; pp 2609–2614, ISBN 978-1-4244-0911-2.
32. Mahl, T.; Hildebrandt, A.; Sawodny, O. Forward kinematics of a compliant pneumatically actuated redundant manipulator. In *2012 7th IEEE Conference on Industrial Electronics and Applications (ICIEA)*. 2012 7th IEEE Conference on Industrial Electronics and Applications (ICIEA), Singapore, Singapore, 18–20 Jul. 2012; IEEE, 2012 - 2012; pp 1267–1273, ISBN 978-1-4577-2119-9.
33. Leng, J.; Yan, X.; Zhang, X.; Huang, D.; Gao, Z. Design of a novel flexible shape memory alloy actuator with multilayer tubular structure for easy integration into a confined space. *Smart Mater. Struct.* **2016**, *25*, 25007, doi:10.1088/0964-1726/25/2/025007.
34. Helps, T.; Vivek, A.; Rossiter, J. Characterization and Lubrication of Tube-Guided Shape-Memory Alloy Actuators for Smart Textiles. *Robotics* **2019**, *8*, 94, doi:10.3390/robotics8040094.
35. Motzki P.; Kunze J.; York A.; Seelecke S. *Energy-efficient SMA Vacuum Gripper System*, 2016.
36. Meier, H.; Czechowicz, A. Computer-Aided Development and Simulation Tools for Shape-Memory Actuators. *Metall and Mat Trans A* **2012**, *43*, 2882–2890, doi:10.1007/s11661-011-1020-5.